Structure and Dynamics of Benzyl-NX3 (X = Me, Et) Trifluoromethanesulfonate Ionic Liquids

ARTICLE *in* THE JOURNAL OF PHYSICAL CHEMISTRY B · JANUARY 2014

Impact Factor: 3.3 · DOI: 10.1021/jp410487a · Source: PubMed

4 AUTHORS, INCLUDING:

Anurag Sunda
Central University of Haryana
10 PUBLICATIONS **33** CITATIONS
SEE PROFILE

Vishal Mahesh Dhavale
Tokyo Institute of Technology
15 PUBLICATIONS **128** CITATIONS
SEE PROFILE

Sreekumar Kurungot
CSIR - National Chemical Laboratory, Pune
112 PUBLICATIONS **1,389** CITATIONS
SEE PROFILE

THE JOURNAL OF PHYSICAL CHEMISTRY B

Article

pubs.acs.org/JPCB

Structure and Dynamics of Benzyl-NX_3 (X = Me, Et) Trifluoromethanesulfonate Ionic Liquids

Anurag Prakash Sunda,[‡] Vishal M. Dhavale,[†] Sreekumar Kurungot,[†] and Arun Venkatnathan*[,‡]

[‡]Department of Chemistry, Indian Institute of Science Education and Research, Pune 411008, India

[†]Physical and Materials Chemistry Division, CSIR-National Chemical Laboratory, Pune 411008, India

Supporting Information

ABSTRACT: Ammonium-based benzyl-NX_3 (X = methyl, ethyl) trifluoromethanesulfonate (TFA) ionic liquids (ILs) are low cost, nontoxic, thermally stable ion-conducting electrolytes in fuel cells and batteries. In the present study, we have characterized the structure and dynamics of these ILs using molecular dynamics (MD) simulations and ionic conductivity using electro-chemical impedance spectroscopy (EIS) at varying temperature and relative humidity (RH). Results from MD simulations predict that cation−cation and cation−anion interactions are stronger in benzyltrimethylammonium (BzTMA) compared to benzyltriethylammonium (BzTEA) that diminish with increase in RH. Further, the BzTMA cations show both C−H/Ph (center of mass of phenyl ring) and cation-Ph interactions whereas BzTEA cations show only strong cation-Ph interactions. The C−H/Ph interactions ($\psi \geq 90°$, $d_{H\text{-}Ph} \leq 4$ Å, $\theta < 50°$ and $d_{C\text{-}Ph} \leq 4.3$ Å) in BzTMA cations increase with RH and are highest at RH = 90%. The cumulative impact of electrostatic, cation/Ph, and C−H/Ph interactions results in lower conductivity of BzTMA-TFA IL compared to BzTEA-TFA IL. The EIS measurements show that the trends in ionic conductivity of ILs at RH = 30 and 90% are qualitatively similar to the Nernst−Einstein conductivity from MD simulations. The ionic conductivity of BzTEA-TFA IL is ∼3 times higher than BzTMA-TFA IL at 353 K and RH = 90%.

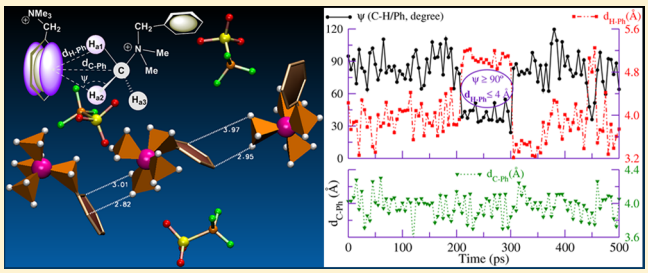

1. INTRODUCTION

Ionic Liquids (ILs) have attained popularity for various electrochemical applications (such as electrolyte in fuel cells, lithium ion batteries and solar cells) in the past decade due to high thermal stability and ionic conductivity.[1−5] Hu and Margulis[6,7] investigated dynamic heterogeneity in ILs and showed that the cationic and anionic diffusivity were highly correlated. Maginn[8] demonstrated the effect of simulation time scale and force-field dependence on accurate determination of transport properties of ILs using atomistic simulations. Angell et al.[9] reviewed the physical properties of protic and aprotic ILs for energy applications. Lu et al.[10] showed improved synthesis, electro-activity and electrochemical properties with use of room-temperature imidazolium-based ILs in π-conjugated polymers. Schmidt et al.[11] studied a Nafion membrane impregnated with imidazolium based ionic liquids and observed less swelling of the membrane without reducing thermal stability. The authors also observed that doping of IL in dry Nafion leads to enhancement of ionic conductivities by 2 orders of magnitude. An application of IL as an electrolyte was also demonstrated by a single molecule electro-chemical gating experiment performed using methylimidazolium trifluoromethanesulfonate by Kay et al.[12] Lu and Archer[13] investigated the potential use of ILs in secondary lithium−metal batteries as hybrid electrolytes.

The use of ammonium based protic and aprotic ILs are of interest as fuel cell electrolytes due to their easy preparation, low cost, performance, excellent thermal stability and ionic conductivity.[14−18] Lee et al.[19] investigated protic ILs such as diethylmethylammonium trifluoromethanesulfonate ([dema$^+$][TFA$^-$]) as a proton conductor in fuel cells and observed fast proton exchange occurs due to the ammonium cation. Di Noto et al.[20−22] studied the influence of anions on proton-conduction of Nafion 117 impregnated with a quaternary ammonium ion based IL. The authors chose tetraethylammonium methanesulfonate, triethylammonium[TEA$^+$] methanesulfonate[TFA$^-$], and triethylammonium[TEA$^+$] perfluorobutanesulfonate [PFBu$^-$] doped Nafion 117 membrane and observed a significant increase in proton conduction, thermal stability, and mechanical properties of the membrane. Sood et al.[23] investigated membrane nanostructure and transport properties of IL [TEA$^+$-TFA$^-$] doped Nafion membrane. The authors observed a substantial increase in anhydrous ionic conductivity with increase in IL concentration.

Chang et al.[24] employed molecular dynamics (MD) simulations on neat and hydrated [dema$^+$][TFA$^-$] IL. The authors observed that hydration leads to enhanced vehicular ionic conductivity. Tsuzuki[25] concluded that cation−anion interaction, shape/symmetry or size of cation, conformational flexibility, and molecular mass play a key role in diffusion of ILs.

Received: October 23, 2013
Revised: January 20, 2014
Published: January 29, 2014

Blanchard et al.[26] studied diffusion mechanism in triethylamine based protic ILs using pulse field gradient stimulated echo NMR spectroscopy. The authors did not find any evidence of Grötthuss mechanism and reported acidic proton diffusion in the presence of water.

While ammonium-based protic and aprotic ILs have been considered as fuel cell electrolytes, their studies have been limited only to room temperature. Further, these ILs have high miscibility with water and leaching even at room temperature that limits their application as dopant in solid polymer membrane electrolytes. To overcome these limitations we have chosen benzyltrimethylammonium triflate (BzTMA-TFA) and benzyltriethylammonium triflate (BzTEA-TFA) ILs in the present study. These ILs are nontoxic,[27] exist in solid form at room temperature with a glass transition temperature >80 °C, and show high thermal stability (>300 °C).[28] These ILs can offer better thermal stability, ionic conductivity, reduced IL leaching, and can enhance the fuel cell operation at higher temperature (>140 °C) by reducing CO poisoning of the Pt catalyst. The objective of this work is to elucidate a qualitative relationship between structure and dynamics of BzTMA-TFA and BzTEA-TFA ILs. Further, influence of temperature (300, 318, 333, and 350 K) and relative humidity (RH = 0, 30, and 90%) on structure and dynamics is also examined. The Nernst−Einstein conductivity of ILs is calculated using MD simulations and ionic conductivity is measured using electrochemical-impedance spectroscopy (EIS). The details of MD simulations are described in Section II. The experimental details are described in Section III. The structural and dynamical properties from MD simulations and experimental studies are presented in Section IV. A summary of the most important results concludes the paper.

2. COMPUTATIONAL SECTION

The chemical structure of BzTMA-TFA and BzTEA-TFA ILs are shown in Figure 1. All MD simulations were performed

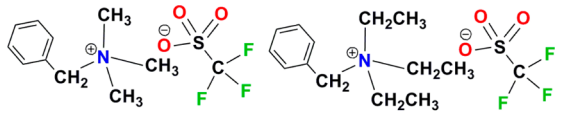

Figure 1. Chemical structure of (a) BzTMA-TFA IL and (b) BzTEA-TFA IL.

using the GROMACS[29] 4.5.4 program. All force-field parameters (except partial charges) of benzyl trimethyl ammonium cation ($BzTMA^+$) and benzyl triethyl ammonium ($BzTEA^+$) cation were taken from the OPLS-AA force-field database.[30] The partial charges of ammonium cations was calculated using Chelp[31] algorithm (MP2/6-31G** basis set) in the Gaussian 03 program[32] (see Figure S1 of Supporting Information). The complete set of force-field parameters for cations is presented in Supporting Information Table S1. The force-field parameters of triflate anion were taken from the work of Sunda et al.[33] The input configurations for MD simulations were obtained as follows: An energy minimized BzTMA-TFA IL molecule was replicated to generate a cubic box of 64 IL molecules. The replicated configuration was heated from 300 to 1000 K and cooled back to 300 K with an annealing time of 6.75 ns. The final configuration from the annealing was used and replicated to generate a cubic box of 512 IL molecules. A similar procedure was applied for BzTEA-TFA IL and these replicated systems were now used as input for MD simulations. MD simulations were performed for BzTMA-TFA and BzTEA-TFA ILs at 300, 318, 333, and 353 K. The leapfrog algorithm[34] was chosen as an integrator with a time step of 1 fs. The cutoff for van der Waals and electrostatic interactions were chosen as 1.0 nm. The long-range electrostatic interactions were described by the Particle-Mesh Ewald (PME) method.[35,36] The input configuration of each ionic IL was used for equilibration for 10 ns using the NPT ensemble with a 1 bar isotropic pressure and a Berendsen barostat.[37] The velocity-rescale thermostat[38] was used to maintain a constant temperature with a coupling time of 0.1 ps. The equilibrated structure were used to perform MD simulation for dry (neat) and aqueous (30 and 90 wt % water) ILs. The SPC/E[39] water model was used to create hydrated ILs. The number of water molecules, box length, and density (calculated from equilibration) of ILs are shown in Supporting Information Table S2. As a benchmark, our simulated density of neat ILs (~1.2 g cm^{-3}, 300 K) is in agreement with the experimental[28] density (1.2 g cm^{-3}, 298 K). Equilibration was followed by a 20 ns production run using the NVT ensemble. The Nosé−Hoover thermostat[40,41] was used with a coupling time of 0.2 ps. The snapshots from the production run (RH = 30 and 90% at 300 and 353 K) are shown in Supporting Information Figure S2. Trajectories generated from the production run were saved every 5 ps for calculation of structural (pair distribution functions, clustering) and dynamical properties (mean square displacement, diffusion).

3. EXPERIMENTAL SECTION

Benzyltrimethylammonium chloride, benzyltriethylammonium chloride, and trifluoromethanesulfonic acid (from Aldrich) were used as received. IL synthesis was carried out by reaction of chloride salt of respective cation with trifluoromethanesulfonic acid (with molar ratio $BzNX_3Cl$/TFA = 1.05; X = Methyl or Ethyl) in deionized water at room temperature in an ice bath (stir for 30−45 min). Subsequently, water was evaporated from the synthesized IL using a rotavap. After removal of water, methanol was added and stirred for 15−20 min followed by filtration to remove impurities or unreacted products. Methanol was evaporated followed by drying at 100 °C under vacuum for 24 h. The synthesized IL was characterized by ^1H, ^{13}C, and ^{19}F NMR and characteristic NMR peaks were observed (see Figure S3 and Figure S4 of Supporting Information). The characteristic $\pi \rightarrow \pi^*$ transition peak of the phenyl group of ILs at 240−275 nm wavelengths was observed in the UV−visible spectrum (see Figure S5 of Supporting Information). The thermal stability of ILs was examined by thermogravimetric analysis (TGA) analyzer where both ILs show thermal stability up to 600 K (see Figure S6 of Supporting Information).

4. RESULTS AND DISCUSSION

Interactions in BzTMA-TFA and BzTEA-TFA ILs. The structural influence of methyl or ethyl substituents attached to the quaternary nitrogen on various interactions between cation−cation and cation−anion is examined by pair distribution functions (PDFs) shown in Figure 2. The strong cation−cation and cation−anion interactions are observed from N−N and N−S PDFs in BzTMA-TFA IL, respectively. The peak position of cation−cation interaction in N−N PDF (see Figure 2a) is shifted from 6.1 to 7.4 Å from methyl to the bulky

dx.doi.org/10.1021/jp410487a | J. Phys. Chem. B 2014, 118, 1831−1838

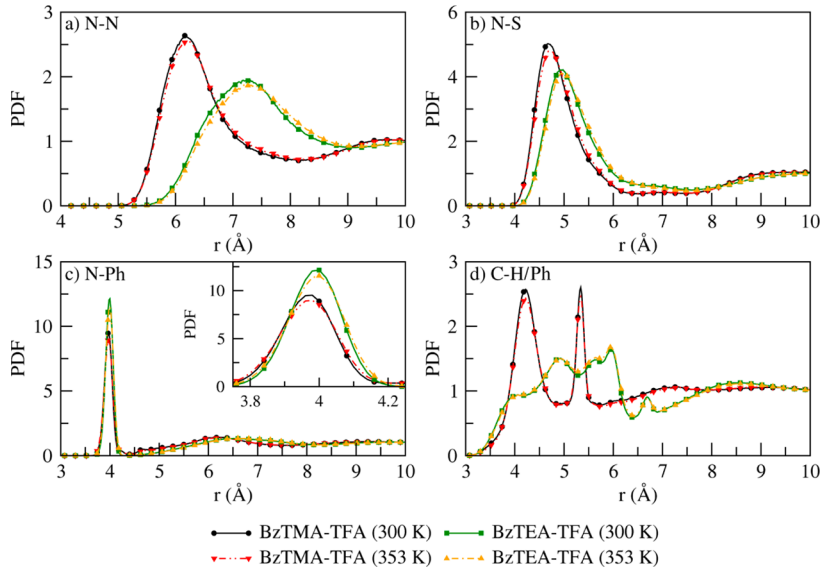

Figure 2. (a) N−N, (b) N−S, (c) N-Ph, and (d) C−H/Ph interactions in neat BzTMA-TFA and BzTEA-TFA IL.

ethyl substituted ammonium cation. The ethyl-substituted ammonium cation shows larger solvation shell of ∼9 Å compared to BzTMA-TFA IL (∼8 Å). Similarly, cation−anion interactions characterized by N−S PDFs, shows a peak position in the N−S PDF at 4.75 Å in BzTMA-TFA compared to 5 Å in BzTEA-TFA IL (see Figure 2b). The N−S PDFs peak at 5 Å is similar to cation−anion interactions in [dema$^+$]-[TFA$^-$] as observed by Chang et al.[24] The influence of aromatic ring (using center of mass of phenyl ring denoted as **Ph**) on structure and cationic interactions is seen from the N-Ph and C−H/Ph PDFs. A sharp peak seen from the N-Ph PDF at 4 Å (see Figure 2c) resembles closely with previously reported work[42−45] on cation/π interactions. The d_{N-Ph} distance (∼4 Å) from the N-Ph PDF peak closely resembles the d_{N-Ph} distance between the aromatic benzene ring and nitrogen atom of NMe_4^+ reported by Reddy and Sastry.[46] In BzTMA-TFA IL, a sharp intense peak at 4.2 Å (see Figure 2d) shows strong C−H/Ph interactions.[47] Ab initio calculations[48−51] have shown that dispersion contributes significantly to C−H/π interaction. However, such interactions could not be seen in BzTEA cations due to less dispersion interactions between the terminal C−H of ethyl group and the phenyl ring. The C−H/Ph interactions completely diminish in BzTEA-TFA IL. This is because the ethyl group (compared to methyl) reduces the positive charge on the nitrogen atom.

This is further examined from the ^{1}H NMR (see Figure 3) spectra, where the CH_2 proton of benzyl group is shielded by 0.1 δppm in BzTEA-TFA compared to BzTMA-TFA. For all PDF, the effect of temperature is also insignificant in both ILs. The effect of RH on anion−anion interaction is insignificant as seen from S−S PDFs (see Figure S7 of Supporting Information). However, a significant effect of RH is observed (see Figure S7 of Supporting Information) for other interactions. For example, the cation−cation, cation−anion and cation−phenyl (N−Ph) interactions decrease significantly at RH = 90% compared to neat (RH = 0%) and RH = 30%. The N-Ph interactions almost disappear at RH = 30% and RH = 90%. In contrast with other interactions, the effect of RH on C−H/Ph interactions shows the following trends: The peak intensity of C−H/Ph PDF increases with RH in BzTMA-TFA IL (see Figure 4a), which suggests hydration leads to an

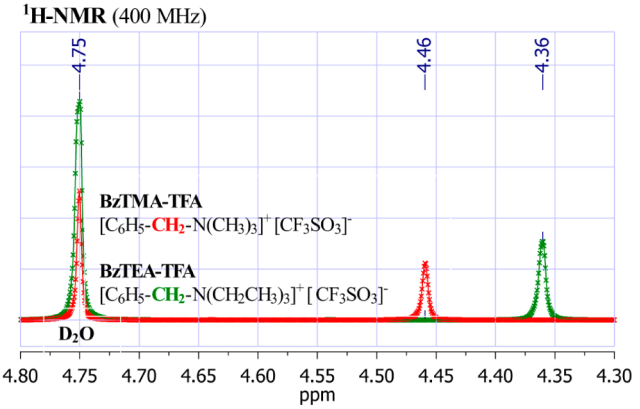

Figure 3. ^{1}H NMR peak shift for CH_2 proton of benzyl group attached to nitrogen atom in BzTMA-TFA (red) and BzTEA-TFA IL (green).

increase in C−H/Ph interactions. However, C−H/Ph interactions are absent even at RH = 90% in BzTEA-TFA (see Figure 4b).

C−H/Phenyl Interaction and Cluster Analysis. The presence of C−H/Ph interactions in BzTMA-TFA IL is examined through a cluster analysis in neat IL (RH = 0%). The clustering of cations and anions in IL is calculated with respect to the center of mass of a reference ion-pair using the Gromos algorithm[52] method with a cutoff distance of 1 nm. Because the neat system is completely homogeneous, the reference ion-pair can be chosen randomly from a box of ion-pairs. An orthographic view of a cluster of IL molecules is shown in Figure 5. A clear view of C−H/π interaction in BzTMA cations (see Figure 5a) where the methyl group of other two neighboring molecules in the cluster shows weak intermolecular noncovalent interactions with the phenyl ring of center BzTMA-TFA IL molecule. As depicted in Figure 5a, the distance between hydrogen atom of methyl group and carbon atoms of the plane of phenyl ring is less than 4 Å. However, such preferred alignment of terminal methyl group with the phenyl ring is not seen in the cluster of BzTEA-TFA IL (see Figure 5b).

dx.doi.org/10.1021/jp410487a | J. Phys. Chem. B 2014, 118, 1831−1838

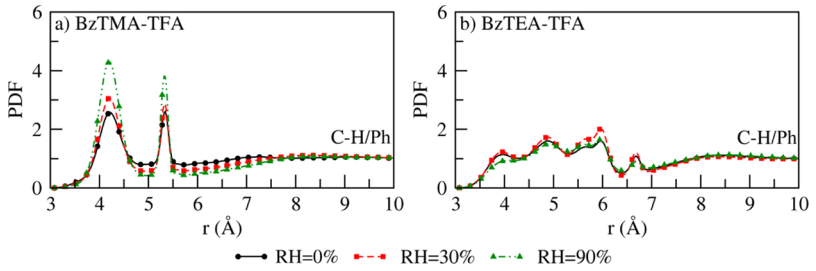

Figure 4. C−H/Ph interactions in neat and hydrated (a) BzTMA-TFA and (b) BzTEA-TFA ILs.

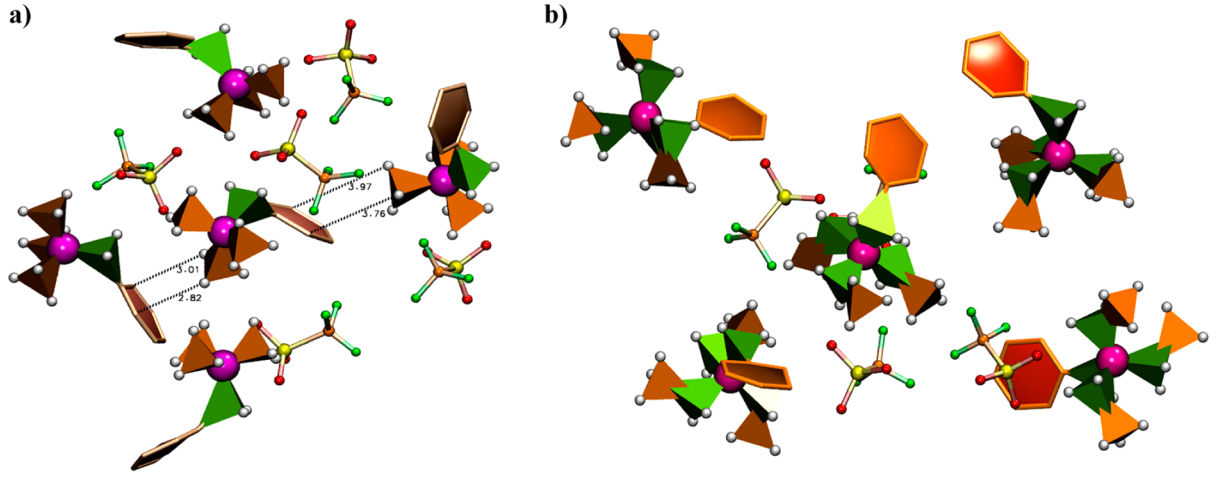

Figure 5. Cluster (orthographic view) of (a) BzTMA-TFA (illustrate C−H/Ph interactions) and (b) BzTEA-TFA ILs respectively. [Nitrogen, CPK (magenta); CH_3, polyhedral (orange); CH_2 carbon, polyhedral (green); aliphatic hydrogen, CPK (white), aromatic ring paper chain and TFA, CPK (sulfer, yellow; oxygen, red; fluorine, green)].

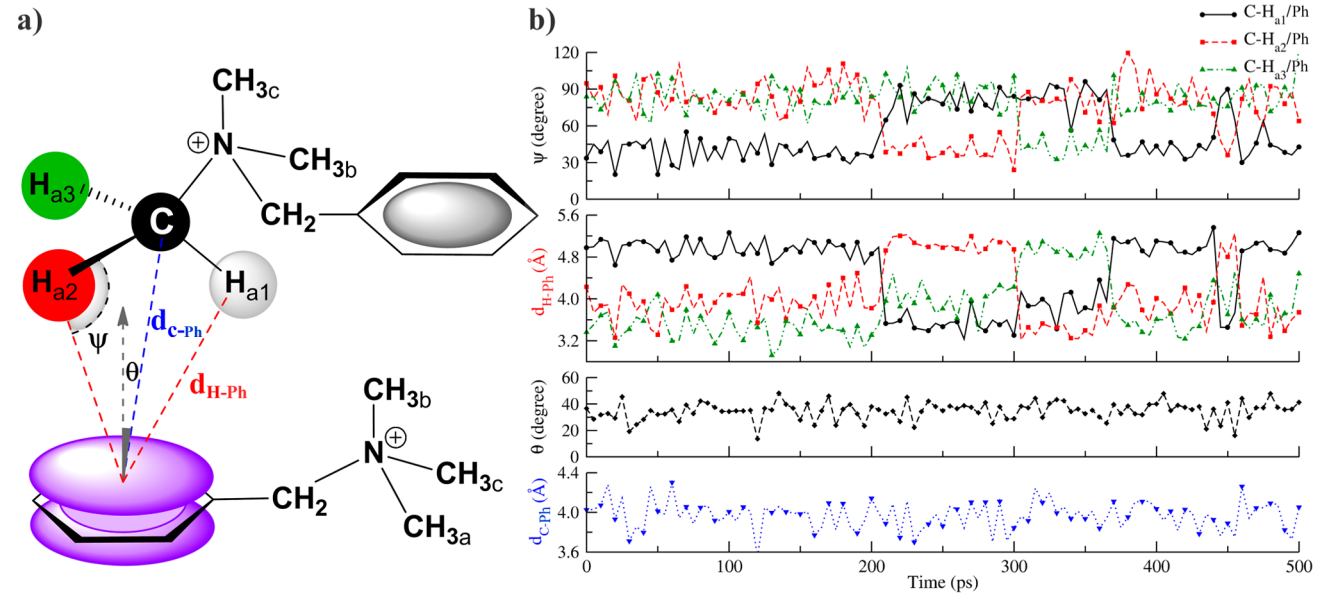

Figure 6. (a) Schematic representation of C−H/Ph interaction in BzTMA cations and (b) variation in C−H/Ph angle (ψ), θ and distances ($d_{H\text{-}Ph}$ and $d_{C\text{-}Ph}$) calculated with time for three methyl hydrogen atoms (H_{a1}, H_{a2} and H_{a3}) and methyl carbon, respectively (where ψ, is the angle between plane of phenyl ring with the H−C vector; θ is angle between methyl carbon atom and vector perpendicular to the plane of phenyl ring).

The directionality and dynamic behavior of C−H/Ph interactions in the cluster of BzTMA-TFA IL is calculated from the final 0.5 ns trajectory of MD simulations at 300 K. To characterize these interactions, a second ion pair is chosen as an average structure that is system and time averaged (includes all ion pairs within the cutoff distance of 1 nm from the reference ion-pair generated by the cluster analysis described earlier). A schematic of C−H/Ph interaction in BzTMA cations between a reference ion-pair and the second ion-pair is shown in Figure 6a. The angle, ψ, denotes the angle formed between the plane of the phenyl ring with the H−C vector. The variation in C−H/Ph angle (ψ) and distances (d_{H-Ph} and d_{C-Ph}) with time is

dx.doi.org/10.1021/jp410487a | J. Phys. Chem. B 2014, 118, 1831−1838

shown in Figure 6b for three methyl hydrogen atoms (H_{a1}, H_{a2}, and H_{a3}) and methyl carbon, respectively. The d_{H-Ph} distance is less than 4.0 Å for the two hydrogen atoms (ψ = 90 to 120°) and greater than 4.5 Å for the third hydrogen atom (ψ < 60°) respectively. The variation in ψ and d_{H-Ph} distance for methyl H-atom with time suggests that two hydrogen atoms of methyl group orient toward the phenyl ring at a time where the ψ changes with rotation of hydrogen atoms. As the angle decreases from 90 to 30°, the methyl hydrogen atom moves away from the plane of the aromatic ring. An average θ (angle between methyl carbon atom and vector perpendicular to the plane of phenyl ring) value is 35°. The average d_{C-Ph} distance is 4.1 Å and is in excellent agreement with the geometric criterion for C−H/π interactions reported by Plevin et al.[47] Ab initio calculations on C−H/π interaction between hydrocarbon and benzene by Tsuzuki et al.[48−50] have shown that the interaction is strongest when a C−H bond of methyl group is pointing directly at the center of the π e^- cloud of aromatic ring (ψ = 180°). Plevin et al.[47] found that the deviation in ψ from 180° slightly reduces the interaction energy and the effect of lateral displacement of the donor group on interaction energy is minimal. The authors had concluded that a "classical XH/π geometry (ψ = 180°) is favored". However, the location of the carbon atom close to the π e^- cloud of phenyl ring determines the interaction energy rather than the location of the proton.[47]

Nernst−Einstein Ionic Conductivity: MD Simulations. The ionic mobility of ILs (for RH = 30 and 90%) is determined from the mean square displacement (MSD) using Einstein relationship.[34] A log MSD versus log time plot and its first derivative (denoted as β) is shown in Figure S9 of Supporting Information. A value of β ∼1 suggests diffusive behavior.[6−8,53,54] For all temperatures and RH = 30 and 90%, the β value is ∼1 suggesting a diffusive regime (2−18 ns). The self-diffusion coefficients (D_A) are calculated from the diffusive regime of MSD (see Figure S10 of Supporting Information).

However, at RH = 0%, β-value deviates significantly from 1 and varies randomly and hence a diffusive behavior could not be achieved. In order to check if diffusive behavior exists, we performed 40 ns production run simulations at 353 K for both ILs. However, a diffusive regime could not be obtained and hence the diffusion coefficients for neat ILs cannot be calculated (see Figure S9 of Supporting Information). The nondiffusive behavior could be due to the solid phase of the neat IL up to 353 K. At RH = 30 and 90%, the conductivity of IL is calculated from diffusion coefficient of cation and anion using Nernst−Einstein relation[55] (see Figure 7). An examination of Nernst−Einstein conductivity (σ_{N-E}) of IL at varying RH and temperature shows the following trends: For all temperature and RH, the σ_{N-E} is slightly higher in BzTEA-TFA IL compared to BzTMA-TFA IL. For example, at 353 K and RH = 30% the σ_{N-E} of BzTEA-TFA IL is higher by a factor of 1.32 compared to the σ_{N-E} of BzTMA-TFA IL. Similar trends are seen at RH = 90%. For both ILs, at all temperatures an increase in σ_{N-E} by an order of magnitude is seen from RH = 30 to 90% (see Figure 7). The cation−anion interactions decrease with RH and hence ionic mobility increases with RH. As expected, for all RH the conductivity of ILs increase with temperature. The trends seen in σ_{N-E} of ILs are compared by the measurement of ionic conductivity using electro-chemical impedance spectroscopy (EIS) as discussed in the next section.

Impedance and Ionic Conductivity: Electrochemical Impedance Spectroscopy. Impedance of ILs is measured using BioLogic Science Instrument and RH is controlled in

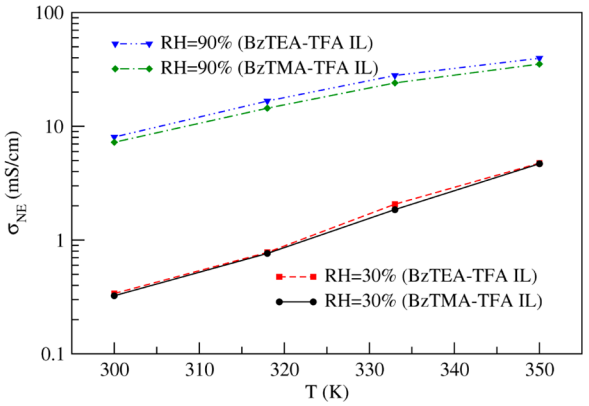

Figure 7. Nernst−Einstein conductivity from diffusion coefficient obtained for ammonium cation and triflate anion (at RH = 30 and 90%) of BzTMA-TFA and BzTEA-TFA ILs.

ESPEC (SH-241) benchtop type temperature and humidity chamber. The AC impedance is measured using two probes method at RH = 30% to RH = 90% and at four temperatures (300, 318, 333, and 353 K). The frequency responses are analyzed by EC-lab software.

The impedance response at 300 and 353 K for both ILs is shown as a Nyquist plot (see Figure 8). The Nyquist plots at 318 and 333 K are shown in Figure S11 of Supporting Information. The resistance of ILs decreases with increase in RH (RH = 30 to 90%) as seen from the high frequency intercept to the real axis of the Nyquist plot. The ionic conductivity calculated as the reciprocal of resistance is shown in Figure 9. As seen, the ionic conductivity is relatively low at room temperature for both ILs. For example, the ionic conductivity is 0.06 and 0.17 mS cm^{-1} for BzTMA-TFA and BzTEA-TFA ILs, respectively (T = 300 K and RH = 30%). The ionic conductivity increases with RH and temperature. At RH = 90% and 353 K, the ionic conductivity of BzTEA-TFA IL is ∼3 times higher compared to the BzTMA-TFA IL. At RH = 90%, electrostatic interactions and cation−phenyl interactions are relatively very low. While, lower molecular mass should result in faster ionic diffusion in BzTMA-TFA ILs, the presence of strong C−H/Ph interactions (see Figure 4a) in BzTMA-TFA IL limits the mobility of ions. This is consistent with the study of Tsuzuki[25] on factors controlling ionic diffusivity in ILs. For each temperature and RH, the ionic conductivity measured from EIS is lower by an order of magnitude compared to σ_{N-E} from MD simulations. This could be due to solubility of solid IL with increase in RH in EIS electrode setup. The differences can also arise from the effect of partial charges on each atom in MD simulations as observed by Zhang and Maginn[55] for condensed phase simulations of ILs. The comparison of ionic conductivities and simulated diffusion coefficients is further examined from trends seen in the activation energy.

Activation Energy (Ea). The activation energy (Ea) calculated using an Arrhenius expression of Nernst−Einstein conductivity (σ_{N-E} from simulation) and ionic conductivity (σ from EIS) is shown in Table 1. Results from MD simulations shows that increase in RH from 30 to 90% leads to a decrease in Ea (σ_{N-E}) by a factor of 2.4 and 2 for BzTMA-TFA and BzTEA-TFA IL, respectively. However, experiments show that the effect of RH on Ea (σ) is significant only for BzTEA-TFA IL compared to BzTMA-TFA IL. For example, the Ea (σ) of BzTEA-TFA IL decreases from 36.24 kJ/mol (RH = 30%) to 19.63 kJ/mol (RH = 90%). The lack of RH dependence on Ea

dx.doi.org/10.1021/jp410487a | J. Phys. Chem. B 2014, 118, 1831−1838

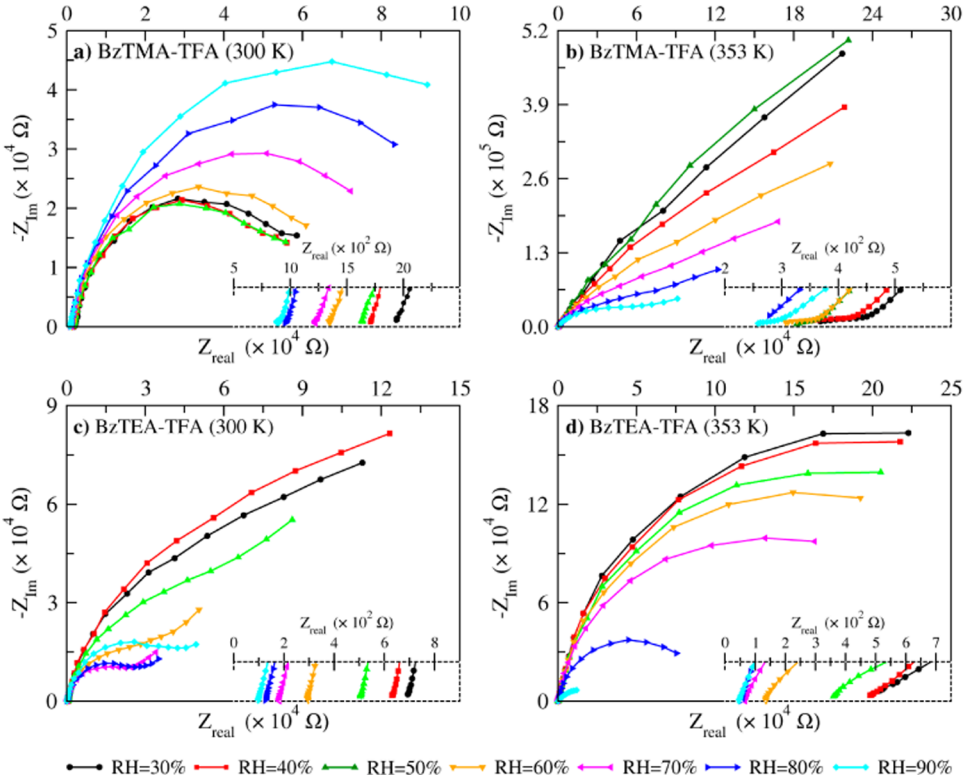

Figure 8. Nyquist plots for BzTMA-TFA IL at (a) 300 K and (b) 353 K and for BzTEA-TFA IL at (c) 300 K and (d) 353 K.

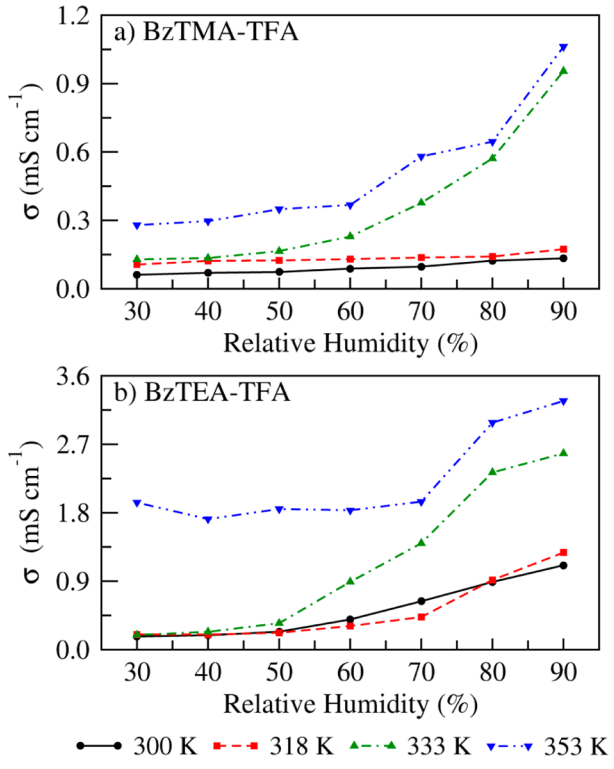

Figure 9. Ionic conductivities measured from EIS for (a) BzTMA-TFA and (b) BzTEA-TFA ILs at varying RH and temperature.

(σ) in BzTMA-TFA IL could be due to the two probe EIS experimental setup where hydration of the solid IL may have not been uniform. However, for both ILs at high RH (90%), the Ea from simulations and experiments are in excellent agreement (difference of ~4 kJ/mol). However, at low RH the differences in activation energy are significant. This difference could be due to a complex temperature dependence (solvation of cations, anions, water network formation)[56] of ion pair domain formation (between simulations and experiment) for each RH.

Table 1. Activation Energy (Ea in kJ/mol) for BzTMA-TFA and BzTEA-TFA ILs, Respectively[a]

	BzTMA-TFA		BzTEA-TFA	
RH %	sim.	expt.	sim.	expt.
30	46.82	23.99	46.79	36.24
40		22.35		34.01
50		25.05		33.08
60		24.37		27.74
70		30.53		22.10
80		23.33		22.57
90	18.75	22.62	23.45	19.63

[a]See Figure S12 and Figure S13 of Supporting Information.

5. CONCLUSIONS

A molecular understanding of structural relation of electrostatic, cation−phenyl (N-Ph), and C−H/Ph interactions with dynamics in BzTMA-TFA and BzTEA-TFA ILs is presented in this study using MD simulation and electro-chemical impedance spectroscopy. In neat BzTMA-TFA IL, strong electrostatic (cation−cation, cation−anion, and anion−anion) interactions are seen compared to BzTEA-TFA IL. The C−H/Ph interactions exist in BzTMA cation, where two hydrogen atoms of any CH_3 group show weak noncovalent interaction with a phenyl ring. The C−H/Ph angle (ψ) fluctuates around 90−120° ($d_{H\text{-}Ph}$ < 4.0 Å) for two hydrogen atoms and around 30° ($d_{H\text{-}Ph}$ > 4.5 Å) for the third hydrogen atom where ψ

dx.doi.org/10.1021/jp410487a | J. Phys. Chem. B 2014, 118, 1831−1838

changes with rotation of hydrogen atoms. As the angle varies from 30 to 90° or higher, the methyl hydrogen atom in BzTMA moves closer to the aromatic ring. However, the C−H/Ph interactions diminish in the BzTEA-TFA IL completely due to the more positive-induced influence of ethyl group on the nitrogen atom. Except for C−H/Ph interaction, the cation−cation, cation−anion, anion−anion, and cation−phenyl interactions decrease with RH.

The TGA of BzTMA-TFA and BzTEA-TFA ILs shows thermal stability up to 600 K and is similar to the thermal stability study of Luo et al.[18] on trioctylammonium triflate or triphenylammonium triflate ILs. The EIS experiments show excellent ionic conductivity of 1.06 mS cm^{-1} (BzTMA-TFA) and 3.27 mS cm^{-1} (BzTEA-TFA), respectively (T = 353 K for RH = 90%). A molecular level understanding of structural and dynamical properties of these ILs from simulations and experiments can facilitate the design of novel protic and aprotic ILs for various technological applications. The role of cationic asymmetry and N−H or N−H/Ph interactions in protic ILs can be the focus of future activities.

■ ASSOCIATED CONTENT

Supporting Information

The complete set of force-field parameters for cations is presented in Table S1. The number of water molecules, box length, and densities are shown in Table S2. The partial charges for cations are shown in in Figure S1. The snapshots at RH = 30% and RH = 90% are shown in Figure S2. The (^{1}H, ^{13}C, and ^{19}F) NMR are shown in Figure S3 and Figure S4. The UV−vis spectra are shown in Figure S5. The TGA is shown in Figure S6. The S−S PDFs that describe anion−anion interactions at 300 K are shown in Figure S7. The effect of RH on cation−cation, cation−anion, and cation−phenyl (N-Ph) PDF profiles at 300 K are shown in Figure S8. For RH = 0 (at 353 K), 30 and 90% (all temperatures), a log MSD versus log time and its first derivative (β) plot for cations, anions, and water is shown in Figure S9. The calculated diffusion coefficients (at RH = 30 and 90%) for cations, anions, and IL are shown in Figure S10. At varying RH, Nyquist plot at 318 and 333 K are shown in Figure S11. The Arrhenius plots for $\sigma_{N\text{-}E}$ (MD simulation) and σ (from EIS) are shown in Figure S12 and Figure S13, respectively. This material is available free of charge via the Internet at http://pubs.acs.org.

■ AUTHOR INFORMATION

Corresponding Author

*E-mail: arun@iiserpune.ac.in. Ph: +91 20 2590-8085. Fax: +91 20 2586-5315.

Notes

The authors declare no competing financial interest.

■ ACKNOWLEDGMENTS

This work used the computing resources provided by Indian Institute of Science Education and Research (IISER), Pune, and Center for Development of Advanced Computing, Pune. Authors thank IISER, Pune, and National Chemical Laboratory (NCL), Pune, for experimental research facilities. A.P.S. acknowledges the University Grants Commission for Senior Research Fellowship and the National Council for Science and Technology Communication for Rajat Jayanti Science Communication Fellowship Award. V.M.D. acknowledges Council of Scientific and Industrial Research (CSIR), New Delhi, for Senior Research Fellowship. Funding: (1) Department of Science and Technology (SB/S1/PC-015/2013) India. (2) Department of Science and Technology, Nanomission (SR/NM/NS-42/2009 and SR/NM/NS-15/2011) India. (3) S.K. acknowledges CSIR, New Delhi, for funding through the HYDEN project (CSC0122).

■ ABBREVIATIONS

BzTMA, benzyl trimethyl ammonium; BzTEA, benzyl triethyl ammonium; TFA, trifluoromethanesulfonate; RH, relative humidity; EIS, electrochemical impedance spectroscopy

■ REFERENCES

(1) Macfarlane, D. R.; Forsyth, M.; Howlett, P. C.; Pringle, J. M.; Sun, J.; Annat, G.; Neil, W.; Izgorodina, E. I. Ionic Liquids in Electrochemical Devices and Processes: Managing Interfacial Electrochemistry. *Acc. Chem. Res.* **2007**, *40*, 1165−1173.

(2) Greaves, T. L.; Drummond, C. J. Protic Ionic Liquids: Properties and Applications. *Chem. Rev.* **2008**, *108*, 206−237.

(3) Bai, Y.; Cao, Y.; Zhang, J.; Wang, M.; Li, R.; Wang, P.; Zakeeruddin, S. M.; Grätzel, M. High-performance Dye-sensitized Solar Cells based on Solvent-free Electrolytes Produced from Eutectic Melts. *Nat. Mater.* **2008**, *7*, 626−630.

(4) Armand, M.; Endres, F.; MacFarlane, D. R.; Ohno, H.; Scrosati, B. Ionic-Liquid Materials for the Electrochemical Challenges of the Future. *Nat. Mater.* **2009**, *8*, 621−628.

(5) Vatamanu, J.; Borodin, O.; Smith, G. D. Molecular Insights into the Potential and Temperature Dependences of the Differential Capacitance of a Room-Temperature Ionic Liquid at Graphite Electrodes. *J. Am. Chem. Soc.* **2010**, *132*, 14825−14833.

(6) Hu, Z.; Margulis, C. J. Heterogeneity in a Room-Temperature Ionic Liquid: Persistent Local Environments and the Red-Edge Effect. *Proc. Natl. Acad. Sci. U.S.A.* **2006**, *103*, 831−836.

(7) Hu, Z.; Margulis, C. J. Room-Temperature Ionic Liquids: Slow Dynamics, Viscosity, and the Red Edge Effect. *Acc. Chem. Res.* **2007**, *40*, 1097−1105.

(8) Maginn, E. J. Atomistic Simulation of the Thermodynamic and Transport Properties of Ionic Liquids. *Acc. Chem. Res.* **2007**, *40*, 1200−1207.

(9) Angell, C. A.; Byrne, N.; Belières, J. -P. Parallel Developments in Aprotic and Protic Ionic Liquids: Physical Chemistry and Applications. *Acc. Chem. Res.* **2007**, *40*, 1228−1236.

(10) Lu, W.; Fadeev, A. G.; Qi, B.; Smela, E.; Mattes, B. R.; Ding, J.; Spinks, G. M.; Mazurkiewicz, J.; Zhou, D.; Wallace, G. G.; MacFarlane, D. R.; Forsyth, S. A.; Forsyth, M. Use of Ionic Liquids for π-Conjugated Polymer Electrochemical Devices. *Science* **2002**, *297*, 983−987.

(11) Schmidt, C.; Glück, T.; Schimdt-Naake, G. Modification of Nafion Membranes by Impregnation with Ionic Liquids. *Chem. Eng. Technol.* **2008**, *31*, 13−22.

(12) Kay, N. J.; Higgins, S. J.; Jeppesen, J. O.; Leary, E.; Lycoops, J.; Ulstrup, J.; Nichols, R. J. Single-Molecule Electrochemical Gating in Ionic Liquids. *J. Am. Chem. Soc.* **2012**, *134*, 16817−16826.

(13) Lu, Y.; Das, S. K.; Moganty, S. S.; Archer, L. A. Ionic Liquid-Nanoparticle Hybrid Electrolytes and their Application in Secondary Lithium-Metal Batteries. *Adv. Mater.* **2012**, *24*, 4430−4435.

(14) Yoshizawa, M.; Xu, W.; Angell, C. A. Ionic Liquids by Proton Transfer: Vapor Pressure, Conductivity, and the Relevance of ΔpKa from Aqueous Solutions. *J. Am. Chem. Soc.* **2003**, *125*, 15411−15419.

(15) Nakamoto, H.; Watanabe, M. Brønsted Acid−base Ionic Liquids for Fuel Cell Electrolytes. *Chem. Commun.* **2007**, 2539−2541.

(16) Belières, J. -P.; Gervasiob, D.; Angell, C. A. Binary inorganic salt mixtures as high conductivity liquid electrolytes for >100 °C fuel cells. *Chem. Commun.* **2006**, 4799−4801.

(17) Belières, J. -P.; Angell, C. A. Protic Ionic Liquids: Preparation, Characterization, and Proton Free Energy Level Representation. *J. Phys. Chem. B* **2007**, *111*, 4926−4937.

(18) Luo, J.; Conrad, O.; Vankelecom, I. F. J. Physicochemical Properties of Phosphonium-based and Ammonium-based Protic Ionic Liquids. *J. Mater. Chem.* **2012**, *22*, 20574−20579.
(19) Lee, S. −Y.; Ogawa, A.; Kanno, M.; Nakamoto, H.; Yasuda, T.; Watanabe, M. Nonhumidified Intermediate Temperature Fuel Cells Using Protic Ionic Liquids. *J. Am. Chem. Soc.* **2010**, *132*, 9764−9773.
(20) Di Noto, V.; Negro, E.; Sanchez, J.-Y.; Iojoiu, C. Structure-Relaxation Interplay of a New Nanostructured Membrane Based on Tetraethylammonium Trifluoromethanesulfonate Ionic Liquid and Neutralized Nafion 117 for High-Temperature Fuel Cells. *J. Am. Chem. Soc.* **2010**, *132*, 2183−2195.
(21) Di Noto, V.; Piga, M.; Giffin, G. A.; Lavina, S.; Smotkin, E. S.; Sanchez, J. -Y.; Iojoiu, C. Influence of Anions on Proton-Conducting Membranes Based on Neutralized Nafion 117, Triethylammonium Methanesulfonate, and Triethylammonium Perfluorobutanesulfonate. 1. Synthesis and Properties. *J. Phys. Chem. C* **2011**, *116*, 1361−1369.
(22) Di Noto, V.; Piga, M.; Giffin, G. A.; Lavina, S.; Smotkin, E. S.; Sanchez, J. -Y.; Iojoiu, C. Influence of Anions on Proton-Conducting Membranes Based on Neutralized Nafion 117, Triethylammonium Methanesulfonate, and Triethylammonium Perfluorobutanesulfonate. 2. Electrical Properties. *J. Phys. Chem. C* **2011**, *116*, 1370−1379.
(23) Sood, R.; Iojoiu, C.; Espuche, E.; Gouanve, F.; Gebel, G.; Mendil-Jakani, H.; Lyonnard, S.; Jestin, J. Proton Conducting Ionic Liquid Doped Nafion Membranes: Nano-Structuration, Transport Properties and Water Sorption. *J. Phys. Chem. C* **2012**, *116*, 24413−24423.
(24) Chang, T. M.; Dang, L. X.; Devanathan, R.; Dupuis, M. Structure and Dynamics of N,N-Diethyl-N-methylammonium Triflate Ionic Liquid, Neat and with Water, from Molecular Dynamics Simulations. *J. Phys. Chem. A* **2010**, *114*, 12764−12774.
(25) Tsuzuki, S. Factors Controlling the Diffusion of Ions in Ionic Liquids. *ChemPhysChem* **2012**, *13*, 1664−1670.
(26) Blanchard, J. W.; Belières, J. -P.; Alam, T. M.; Yarger, J. L.; Holland, G. P. NMR Determination of the Diffusion Mechanisms in Triethylamine-Based Protic Ionic Liquids. *J. Phys. Chem. Lett.* **2011**, *2*, 1077−1081.
(27) Frade, R. F.; Afonso, C. A. Impact of Ionic Liquids in Environment and Humans: An Overview. *Hum. Exp. Toxicol.* **2010**, *29*, 1038−1054.
(28) Kulkarni, P. S.; Branco, L. C.; Crespo, J. G.; Nunes, M. C.; Raymundo, A.; Afonso, C. A. M. Comparison of Physicochemical Properties of New Ionic Liquids Based on Imidazolium, Quaternary Ammonium, and Guanidinium Cations. *Chem.—Eur. J.* **2007**, *13*, 8478−8488.
(29) Hess, B.; Kutzner, C.; van der Spoel, D.; Lindahl, E. GROMACS 4: Algorithms for Highly Efficient, Load-Balanced, and Scalable Molecular Simulation. *J. Chem. Theory Comput.* **2008**, *4*, 435−447.
(30) Jorgensen, W. L.; Maxwell, D. S.; Tirado-Rives, J. Development and Testing of the OPLS All-Atom Force Field on Conformational Energetics and Properties of Organic Liquids. *J. Am. Chem. Soc.* **1996**, *118*, 11225−11236.
(31) Chirlian, L. E.; Francl, M. M. Atomic Charges Derived from Electrostatic Potentials: A Detailed Study. *J. Comput. Chem.* **1987**, *8*, 894−905.
(32) Frisch, M. J.; Trucks, G. W.; Schlegel, H. B.; Scuseria, G. E.; Robb, M. A.; Cheeseman, J. R.; Zakrzewski, V. G.; Montgomery, J. A.; Stratmann, R. E., Jr.; Burant, J. C.; Dapprich, S.; Millam, J. M.; Daniels, A. D.; Kudin, K. N.; Strain, M. C.; Farkas, O.; Tomasi,J.; Barone, V.; Cossi, M.; Cammi, R.; Mennucci, B.; Pomelli, C.; Adamo, C. Clifford, S.; Ochterski, J.; Petersson, G. A.; Ayala, P. Y.; Cui, Q.; Morokuma, K.; Malick, D. K.; Rabuck, A. D.; Raghavachari, K.; Foresman, J. B.; Cioslowski, J; Ortiz, J. V.; Stefanov, B. B; Liu, G.; Liashenko, A.; Piskorz, P.; Komaromi, I.; Gomperts, R.; Martin, R. L.; Fox, D. J.; Keith, T.; Al-Laham, M. A.; Peng, C. Y.; Nanayakkara, A.; Gonzalez, C. ;Challacombe, M.; Gill, P. M. W.; Johnson, B.; Chen, W.; Wong, M. W.; Andres, J. L.; Gonzalez, C.; Head-Gordon, M.; Replogle, E. S.; Pople, J. A. *Gaussian 03*, rev. D1; Gaussian Inc.: Pittsburgh, PA, 2003.
(33) Sunda, A. P.; Venkatnathan, A. Molecular Dynamics Simulations of Triflic Acid and Triflate Ion/Water Mixtures: A proton Conducting Electrolytic Component in Fuel Cells. *J. Comput. Chem.* **2011**, *32*, 3319−3328.
(34) Allen, M. P.; Tildesley, D. J. *Computer Simulations of Liquids*; Oxford Science Publications: New York, 1987.
(35) Darden, T.; York, D.; Pedersen, L. Particle Mesh Ewald: An N -log(N) Method for Ewald Sums in Large Systems. *J. Chem. Phys.* **1993**, *98*, 10089−10092.
(36) Essmann, U.; Perera, L.; Berkowitz, M. L.; Darden, T.; Lee, H.; Pedersen, L. G. A Smooth Particle Mesh Ewald Method. *J. Chem. Phys.* **1995**, *103*, 8577−8592.
(37) Berendsen, H. J. C.; Postma, J. P. M.; DiNola, A.; Haak, J. R. Molecular Dynamics with Coupling to an External Bath. *J. Chem. Phys.* **1984**, *81*, 3684−3690.
(38) Bussi, G.; Donadio, D.; Parrinello, M. Canonical Sampling through Velocity Rescaling. *J. Chem. Phys.* **2007**, *126* (014101), 1−7.
(39) Berendsen, H. J. C.; Grigera, J. R.; Straatsma, T. P. The Missing Term in Effective Pair Potentials. *J. Phys. Chem.* **1987**, *91*, 6269−6271.
(40) Nosé, S. A Molecular Dynamics Method for Simulations in the Canonical Ensemble. *Mol. Phys.* **1984**, *52*, 255−268.
(41) Hoover, W. G. Canonical Dynamics: Equilibrium Phase Space Distributions. *Phys. Rev. A* **1985**, *31*, 1695−1697.
(42) Dougherty, D. A. Cation-π Interactions in Chemistry and Biology: A New View of Benzene, Phe, Tyr, and Trp. *Science* **1996**, *271*, 163−168.
(43) Ma, J. C.; Dougherty, D. A. The Cation-π Interaction. *Chem. Rev.* **1997**, *97*, 1303−1324.
(44) Cubero, E.; Luque, F. J.; Orozco, M. Is Polarization Important in Cation-π Interactions? *Proc. Natl. Acad. Sci. U.S.A.* **1998**, *95*, 5976−5980.
(45) Mahadevi, A. S.; Sastry, G. N. Cation-π Interaction: Its Role and Relevance in Chemistry, Biology, and Material Science. *Chem. Rev.* **2013**, *113*, 2100−2138.
(46) Reddy, A. S.; Sastry, G. N. Cation [M = H^+, Li^+, Na^+, K^+, Ca^{2+}, Mg^{2+}, NH_4^+, and NMe_4^+] Interactions with the Aromatic Motifs of Naturally Occurring Amino Acids: A Theoretical Study. *J. Phys. Chem. A* **2005**, *109*, 8893−8903.
(47) Plevin, M. J.; Bryce, D. L.; Boisbouvier, J. Direct Detection of CH/π Interactions in Proteins. *Nature Chem.* **2010**, *2*, 466−471.
(48) Tsuzuki, S.; Honda, K.; Uchimaru, T.; Mikami, M.; Tanabe, K. The Magnitude of the CH/π Interaction between Benzene and Some Model Hydrocarbons. *J. Am. Chem. Soc.* **2000**, *122*, 3746−3753.
(49) Tsuzuki, S.; Honda, K.; Uchimaru, T.; Mikami, M.; Tanabe, K. Origin of the Attraction and Directionality of the NH/π Interaction: Comparison with OH/π and CH/π Interactions. *J. Am. Chem. Soc.* **2000**, *122*, 11450−11458.
(50) Tsuzuki, S.; Honda, K.; Uchimaru, T.; Mikami, M.; Fujii, A. Magnitude and Directionality of the Interaction Energy of the Aliphatic CH/π Interaction: Significant Difference from Hydrogen Bond. *J. Phys. Chem. A* **2006**, *110*, 10163−10168.
(51) Tsuzuki, S. CH/π interactions. *Annu. Rep. Prog. Chem., Sect. C Phys. Chem.* **2012**, *108*, 69−95.
(52) Daura, X.; Gadermann, K.; Jaun, B.; Seebach, D.; van Gunsteren, W. F.; Mark, A. E. Peptide Folding: When Simulation Meets Experiment. *Angew. Chem., Int. Ed.* **1999**, *38*, 236−240.
(53) Morrow, T. I.; Maginn, E. J. Molecular Dynamics Study of the Ionic Liquid 1-n-Butyl-3-methylimidazolium Hexafluorophosphate. *J. Phys. Chem. B* **2002**, *106*, 12807−12813.
(54) Yan, T.; Burnham, C. J.; Del Pópolo, M. G.; Voth, G. A. Molecular Dynamics Simulation of Ionic Liquids: The Effect of Electronic Polarizability. *J. Phys. Chem. B* **2004**, *108*, 11877−11881.
(55) Zhang, Y.; Maginn, E. J. A Simple AIMD Approach to Derive Atomic Charges for Condensed Phase Simulation of Ionic Liquids. *J. Phys. Chem. B* **2012**, *116*, 10036−10048.
(56) Zhang, L.; Xu, Z.; Wang, Y.; Li, H. Prediction of the Solvation and Structural Properties of Ionic Liquids in Water by Two-Dimensional Correlation Spectroscopy. *J. Phys. Chem. B* **2008**, *112*, 6411−6419.